Highly Luminescent Colloidal CdS Quantum Dots with Efficient Near-Infrared Electroluminescence in Light-Emitting Diodes

WILEY-VCH

DOI: 10.1002/ ((please add manuscript number)) draft 6: 10-12-2014
Article type: Full Paper (Advanced Functional Materials)

Efficient Near-Infrared Electroluminescence from Colloidal CdS Quantum Dots in Light-Emitting Diodes

Ashu K. Bansal, Francesco Antolini, Shuyu Zhang, Lenuta Stroea, Luca Ortolani, Massimiliano Lanzi, Emanuele Serra, Sybille Allard, Ullrich Scherf and Ifor D. W. Samuel*

Dr. A. K. Bansal, Dr. S. Zhang, Prof. I. D. W. Samuel
Organic Semiconductor Centre, SUPA, School of Physics and Astronomy, University of St Andrews, St Andrews, KY16 9SS, UK
E-mail: idws@st-andrews.ac.uk
Dr. F. Antolini, Dr. L Storea
ENEA UTTMATF, Via Ravegnana 186, 48018 Faenza (RA), Italy
Dr. L. Ortolani
Electron Microscopy Group – CNR IMM Bologna, Italy
Dr. M. Lanzi
Department of Industrial Chemistry, University of Bologna, Bologna, Italy
Dr. E. Serra
ENEA-UTTMAT, C.R. Casaccia, via Anguillarese 301, 00123 Roma, Italy
Dr. S. Allard, Prof. U. Scherf
Institut für Polymertechnologie Bergische Universität Wuppertal, Gauss-Strasse 20, 42097 Wuppertal, Germany

Keywords: solution processed, hybrid OLED, colloidal qds, CdS, PLQY

Abstract: Quantum dots are of growing interest as emissive materials in light-emitting devices. We report efficient electroluminescence in the near infrared from solution processed hybrid light emitting diodes (LEDs) based on colloidal cadmium sulfide (CdS) quantum dots embedded in an organic semiconductor matrix forming a nanocomposite active layer. We show the highest photoluminescence quantum yield of 69% in solutions and 34% in neat thin films for organic capped colloidal CdS nanoparticles in the near infrared range. We also discuss the device structure and role of the doped active layer in efficiency improvement. With optimized active layer thickness and concentration of QDs, the device exhibits an external electroluminescence quantum efficiency of 0.62% at a peak emission wavelength of

760 nm, providing a route to solution processable flexible light sources for biosensors and medicine.

1. Introduction:

Colloidal quantum dots (QDs) are an attractive choice for next generation optoelectronic devices due to their appealing physical properties of size-tunable band gaps, good photostability, photoluminescence efficiency and compatibility with solution-processing methods[1-3]. Among reported applications, QDs have been actively investigated for light-emitting diodes (LEDs)[4], photodetectors[5], solar cells[6] and bio-labeling[7] as well as down-converters in backlit displays[8]. Recently visible quantum dot based OLED using CdSe/CdS core-shell nanocrystals were reported with record external quantum efficiency (EQE) of 18% and peak emission at 620 nm[9]. In order to explore their potential for biomedical and sensing applications, efforts have been made to extend the optical response of colloidal quantum dots from the visible to the near infrared (NIR) using nanocrystals based on, e.g. CdSe, CdTe and PbS[10, 11]. The efficiency of solution processed OLEDs in NIR emission is very low[12] and there is a large gap in reported performance between the impressive visible results and NIR devices. Organic molecule/nanocrystal hybrid devices were reported recently having core-shell nanocrystals in the NIR range with EQE up to 0.4% with peak emission at 884 nm and maximum 2% with peak emission at 1054 nm[13]. Colloidal quantum dots capped by organic ligands are simple to make and widely studied, but also have low efficiency in the infra-red. For example PbS capped with oleic acid, the electroluminescence peaks at 1250 nm, and has an efficiency of just 1.1%[14]. EQEs of these devices are limited by the photoluminescence quantum yield (PLQY) of QDs in a thin film which is less than 10%, so if QDs with higher PLQY can be developed, EQEs should proportionately increase. Still to our knowledge there is no systematic report available on the

development of efficient colloidal QDs based OLED emitting in the wavelength range 700-900 nm, which is known as the therapeutic window[15] for biological applications.

In this article we report an advance in PLQY and external EQE for NIR emission based on ligand-capped CdS quantum dots. We explore ligand-capped materials for two reasons. First, they are simple to prepare, and second, we found surprisingly high emission in the NIR region of the spectrum. In particular we have exploited the formation of efficient surface trap emission in tri-n-octylphosphine oxide (TOPO) capped CdS QDs and surprisingly show that it can lead to efficient emission for the fabrication of a hybrid LED. We fabricated hybrid LEDs and compared two device architectures: one contains a monolayer of QDs, the other places the QDs in an organic host matrix. The resulting electroluminescence was due either to direct carrier injection into QDs followed by exciton formation and recombination on the QD, or to exciton formation in organic films followed energy transfer to the QDs [7]. Our results show that for ligand-capped QDs higher efficiency is obtained for devices using an organic host matrix than for those using a monolayer of QDs.

2. Results and Discussions

2.1 Photophysical Characterisation of Quantum Dots:

The synthesis of the single source precursor Cd bis-octanethiol ($Cd[S(CH_2)_7CH_3]_2$) has been carried out using the protocol proposed by Rees et al. [16] with minor modifications as shown in scheme 1 in the experimental section. A schematic representation of colloidal TOPO capped CdS QDs after the thermolysis of the cadmium bis-octanethiolate precursor performed in the presence of a coordinating solvent (tri-n-octylphosphine oxide, TOPO) is shown in Fig. 1. The growth of the QDs was carried out in a reaction flask at elevated temperature at 220-270 °C and the time course growth dynamics of the QDs were monitored at different reaction times. Figure 1 shows absorbance and photoluminescence of such TOPO capped QDs at various reaction times. The absorption spectra show a well defined shift in the band edge

absorption at various reaction temperatures and all QDs absorb below 420 nm. For example as shown in fig.1a the band edge absorbance of the QDs move from 340 nm at 30 minutes reaction time to 380 nm after a reaction time of 240 minutes at a temperature of 220 °C. These particular QDs did not show any band edge emission when excited in solutions at 350 nm, but emitted at longer wavelength, a broad emission with peak up to 790 nm in the near infrared (NIR) as shown in fig.1b. The PL maxima shift toward red as a function of baking time within the interval 640 – 790 nm shows the dependence of the PL properties on the QDs size.

Surprisingly these CdS QDs are highly emissive, the photoluminescence quantum yield (PLQY) was measured using integrating sphere and values of PLQY obtained are shown in fig. 1. The time course of the PLQY shows a rapid increase a maximum to 68.9% during the first 90 minutes then a decreases to 37% upon further heating. The high PLQY is surprising considering that QDs are obtained with the use of an organic ligands system trioctylphosphine/trioctylphosphine oxide (TOP/TOPO). In literature CdS QDs have been reported to emit at these longer wavelengths if the surface of the nanocrystals is not passivated completely but non-radiative recombination due to the associated defect states leads to very weak emission with less than 1% PLQY[17]. High PLQY has been reported eariler in CdTe QDs using thiol ligands[18] where authors suggest that the PLQY is function of the steric hindrance of the ligand.

Figure 2a shows the size distribution of the CdS QDs as a function of the annealing time together with the full width at half maximum (FWHM). The size of the CdS QDs was determined using the equation proposed by Yu et al[19]. In the initial period (30 – 90 minutes), there is a rapid enhancement of the size of CdS QDs followed by a slower growth during 120–240 min as soon as the precursor decomposed. This trend correlates with the classical La Mer model of nucleation and growth followed by the Ostwald ripening where the larger particles are formed at the expense of the smaller ones[20, 21]. The FWHM, direct

indicator of the particle size distribution, follows a similar trend: distribution of the particle size in the first 90 minutes increases rapidly (FWHM from 1 nm to 1.12 nm) and then oscillates around the value of 1.20 nm during 150 – 240 min growth dynamics. This size defocusing that follows the particle size enhancement confirms the role of the Ostwald ripening after the rapid growth[21]. Figure 2b shows the TEM image of the CdS QDs showing the maximum PLQY on the carbon grid. The image show a homogenous distribution of nanoparticles. There are QDs composed of very small clusters of diameter below 3 nm, and a population of slightly bigger nanoparticles, where the crystal structure is clearly evident. The particle sizes are similar to as obtained by other methods.

In order to understand the formation of such highly emissive QDs, we have done a detailed photophysical studies of various ligands on the QDs. It is well known that the optical properties of the QDs and their PL quantum yield are strictly correlated with surface ligands. The role of the ligands is to modulate the surface defects of QDs. The dangling bonds on the exposed surfaces of the QDs can be passivated by the ligands and the deep trap emission states can be consequently modulated[22]. In metal chalcogenide QDs, chalcogen filled states and metal derived empty states can lead to mid gap states which work as an ideal passivation system for both of them[23]. The effect of the ligands on photophysical properties and in particular on PLQY is reported for several type of II-VI QDs and in particular for CdTe[18, 24, 25] and CdSe[26-28].

In the system presented here the CdS QDs were synthesised form a single source precursor (SSP) with a solvothermal synthesis process in the presence of TOP and TOPO which acts as ligands and as well as a good solvent for precursor. As the photophysical properties of the QDs depend upon the growth conditions and surface ligands, the combined effect of PL emission at longer wavelength coupled with a high PLQY has been investigated by changing the solvent and the ligand type in the reaction synthesis. The synthesis of the CdS

was carried out both on TOPO, a coordinating sovent and octadecene ODE, a non-coordinating solvent using TOP and diphenylphosphine (DPP) in the reaction media and changing their ratio with respect to the CdS single source precursor. Figure 3a shows that a high value of PLQY is obtained only when the synthesis is carried out in the presence of TOPO coupled with TOP and DPP in comparison to non-coordinating solvent such as ODE or in pure TOPO. When TOP is used the PLQY is dependent on the amount of this reagent while in the case of DPP the PLQY is practically high and constant for most of the interval. These results point out the importance of TOP and DPP coupled with TOPO to obtain a high PLQY. The effect of TOP and DPP on the synthesis of CdSe QDs has been recently higlighted by several authors[29, 30]. In these works it is reported that TOP is not the key reagent for an high yield, but the dioctylphosphine (DOP) that is present in as an impurity in the TOP, plays a key role. The effect of DPP is similar to that of DOP and its effect on the PLQY of QDS has been highlighted[30]. As DPP is a more reactive species than TOP, there is no need to add it in large excess, so a ratio of unity is enough to obtain the desired enhancement of PLQY.

Figure 3b shows the shift of the PL maxima of the QDs as a function of TOP (or DPP)/SSP ratio in both solvents. The figure shows that in ODE, both TOP and DPP have no effect on PL maxima: the wavelength of emission is 543 nm in both cases in comparison to the value of 585 nm found in pure ODE without any ligand. As for the PLQY in TOPO both TOP and DPP shift the PL maxima toward longer wavelength (figure 3b). The effect of concentration is also observeable when TOP is used. When the ratio of the TOP/SSP moves from 1 to 3 the PL maxima shifts from 553 nm to 706 nm and then it remains practically constant at higher ratios. In the case of DPP the PL maxima emission still remains the same for all the ratios of DPP/SSP even if its absolute value is slightly lower with respect to the one reached with TOP (676 nm instead of 715 nm for TOP with a ligand/precursor ratios of 30).

These results suggests that the DOP impurity in TOP is a crucial molecule in PLQY enhancement and wavelength shift in the CdS QDs synthesis in TOP/TOPO. However the

action of di-alkyl(aryl)-phosphines have to be coupled with the presence of TOPO to be effective. This further evidence suggests a complex mechanism of QD growth with specific optical properties involving dialkyl(aryl)-phospines, TOPO and probably its impurities such as di-n-octylphospine oxide (DOPO) and di-n-octylphospinic acid (DOPA) [31, 32].

The behaviour of QDs in solid state samples was also studied where thin films of QDs were prepared by spin-coating the solutions at 1200 rpm on quartz substrates. The absorption and photoluminescence properties of the QDs are shown in supplementry information at two different annealing times. The results show the same behaviour as in solution. The photoluminescence quantum yield of neat films of our QDs was measured using an integrating sphere. The nanocrystals show PL quantum yield up to 34% which to our knowledge is the highest value from colloidal QDs passivated by organic molecules in the NIR range.

2.2 Devices Characterisation:

The device architecture with corresponding energy levels of various layers is shown in Fig. 4, in which the electrode work functions and the HOMO/LUMO energies for PEDOT, PVK, CdS QDs[33], o-DBFPPO and B3PyMPM are taken from the literature[34, 35]. Three different sets of devices were fabricated. In set 1, the device structure contained a monolayer of QDs - ITO/PEDOT:PSS (40 nm)/PVK (35 nm)/QD (10 nm)/B3PyMPM (60 nm)/Ca (20nm)/Al (100nm). In set 2, instead of QDs alone, a blend of QDs with CBP in a volume ratio of (0.05:0.95) was used. In set 3, a blend of QDs with o-DBFPPO in a volume ratio of (0.05:0.95) was used, with the other layers the same as for sets 1 and 2. In all three types of devices, the EL spectrum is very similar to the PL spectrum as shown in figure 4. It shows only emission from the QDs with a broad peak at 760 nm. It is important to note that no host emission was visible from either of the blends implying either complete energy transfer from host to the QDs or direct excitation formation on the QDs.

Fig. 5a shows the external quantum efficiency of all three sets of devices. For set 1 (monolayer of QDs), the EQE is less than 0.2% in comparison to set 2 (QD:CBP blend) where EQE reaches to 0.62%. In device set 3, EQE is low and less than 0.2%. Fig 5b shows the current-voltage-light output characteristics for all three set of devices. The turn on voltage for device set 1 is above 25 V, which reduces drastically in device set 2 to 15 V and in device set 3 even reduces further to just less than 10 V. The low EQE and very high turn on voltage in the case of device set 1 suggest insufficient charge transport when the excitons are directly formed in a monolayer of QDs. The energy level diagram shown in fig. 4 shows that the HOMO level of PVK is at 5.5 eV, so there is a large energy step for hole injection from this layer into the QDs which have a HOMO energy level at 6.3 eV. In contrast, there is not a barrier to electron injection. This large difference in the injection barriers for electrons and holes into the QDs results in a carrier imbalance that leads to the low efficiency of the devices made from the neat film. The carrier imbalance may also be due to quenching of excitons by the injected charge[36]. The blending of QDs with host materials improves the charge injection as this process reduces the energy level step and can improve the efficiency. The implication of this is that excitons will not form directly on the QDs. As seen in figure 5a, device set 2, which uses a CBP host, an ambipolar host material, improves the efficiency to 0.62%. This improvement in efficiency in CBP devices is due to the reduced barrier to hole injection into the light-emitting layer as the HOMO energy of CBP is 5.95 eV, closer to that of PVK. In contrary the efficiency does not improve in device set 3 where o-DBFPPO, an electron transport material, is used whose HOMO level (5.96 eV) is similar to CBP, although it reduces the turn on voltage substantially as shown in fig 5b. Two factors which contribute to the higher current and lower turn-on voltage in the o-DBFPPO devices are higher electron mobility and lower barrier to electron injection as its LUMO level is 2.8 eV in comparison to the LUMO level of CBP which is 2.6 eV. Even for CBP host devices, hole injection is limited by a high-energy barrier of 0.45 eV and the resulting charge imbalance explains why

the external efficiency is much lower than might be expected for the high PLQY. These results suggest the performance of the devices can be optimized further if the charge transfer can be balanced.

3. Conclusions

In summary, we have demonstrated the use of colloidal quantum dots as efficient electroluminescent materials in organic light-emitting diodes in the biological tissue window of 700-900 nm. We have reported the highest PLQY of 34% for neat ligand-capped QDs in thin film and 69% in solutions in the near infrared regions, and achieve this using TOPO capped CdS QDs. [31, 32](these references will come out) By utilizing a solution processable multilayer device, electroluminescence has been observed, and an EL quantum efficiency up to 0.62% is achieved. Our results show that broad long wavelength emission produced by colloidal cadmium sulfide QDs can be useful to fabricate near infrared light-emitting devices.

4. Exprmental Section

Synthesis of Cadmium bis-octanthiol precursor: An amount of 1.83 gr of $CdCl_2$ (10 mmol) has been dissolved in 100 ml of water/EtOH 1:1 (v:v), then a volume of NH_4OH 35 % is added until a white suspension disappears (approximately 10-11 ml of ammonium hydroxide solution) and the solution become clear again. In the $CdCl_2$ solution a volume of 3.47 ml of octanthiol (20 mmol) is added drop by drop. A white precipitate is immediately formed and the solution is then leaved to stir for two hour at RT. The precipitate is centrifuged at 4000 rpm for 10 minutes then the powder is resuspended in water /EtOH 1:1 (v:v) again and centrifuged at 4000 rpm for 10 minutes. This washing procedure is repeated twice. The white powder is finally dried O.N. in air (yield 85 %).

$$CdCl_2 + 2\ CH_3(CH_2)_7SH \xrightarrow[RT]{EtOH/H_2O} Cd[S(CH_2)_7CH_3]_2 + 2H^+ + 2\ Cl^-$$

Scheme 1

Elem. analysis: Calculated for $C_{16}H_{34}CdS_2$: Cd, 27.9%; C, 47.7%; H, 8.5%; S, 15.9%; O, 6.26%. Found: Cd, 24.92%; C, 47.95%; H, 8.76%; S, 15.98%.

FTIR (KBr, cm^{-1}): 2955 (antisymmetric stretching -CH3); 2921 (antisymmetric str. -CH2-); 2872 (symmetric str. -CH3); 2849 (symmetric str. -CH2-); 1466 (-CH2- deformation); 1378 (-CH3 deformation); 722 (-CH2- rocking); 647 (C-H deformation).

NMR

The NMR analysis was carried out in the solid state because the compound is insoluble ^{13}C (^{1}H) CPMAS solid state spectrum MAS speed 25 KHz, T = ambient.

The expected resonances are 8 but the signals seem to be the double. This phenomenon could be ascribed to the presence of two different phases (crystalline and amorphous) on the powder. Starting from the methyl group (C8) to the methylene $–CH_2$- bound to the S atom the chemical shifts are: 15.07 ppm (C8 -CH_3), 24.52 ppm (C7 -CH_2-), 28.25 ppm (C6 –CH_2-), 30.51 ppm (C5 –CH_2-), 32.75 ppm (C4 –CH_2-), 34.92 ppm (C3 –CH_2-), 39.07 ppm (C2 –CH_2-), 41.62 ppm (C1 –CH_2-)

Time course of CdS formation: A three necks flask of 50 ml has been loaded with 24 g of TOPO. The powder has been heated at 120° under vacuum (50 mbar) and stirring for 30 minutes, then the solvent has been brought at 220° C under nitrogen for additional 30 minutes. A solution of TOP/cadmium bis-octanthiol has been prepared resuspending 480 mg of Cd-bis octanthiol in 15.4 ml of TOP (the mole ratio between TOP/precursor is set at 29) under nitrogen and stirring for one hour. The TOP/precursor solution is injected into the hot TOPO. After the injection the temperature drops down to 180° C, then the heater is switched to max temperature and within 5-10 min the temperature is stabilised to 220°C. Starting from this moment a volume of 5 ml of the reaction mix has been taken time by time to study the time course of the CdS QDs formation. A volume of 5 ml has been kept at 30, 60, 75, 90, 120, 150, 180 and 240 minutes and the reaction was stopped cooling the solution at RT.

The solution is then poured in 45 ml of acetone and kept at -20°C for 20 minutes to help the precipitation of the QDs. The QDs were recovered by centrifuging the suspension at 4000 rpm for 20 minutes. The pellet is dissolved in 200 μl of chloroform and distributed in two eppendorfs. A volume of 1.2 ml of acetone has been added to each eppendorf to further precipitate and purify the QDs. The solution is then centrifuged at 14.000 rpm for 10 minutes. The dissolution/precipitation step has been repeated twice. Finally the pellet is re-dissolved in 0.5 ml of chloroform for the final optical and structural characterisation.

Effect of TOP/DPP on CdS QDs optical properties.

In a typical reaction an amount of 20.5 mg of Cd-bis- octanthiol (0.05 mmol) was loaded in a pyrex tube. A volume of 3 ml of ODE (previously degassed under vacuum, 50 mbar, at 120° for 30 min, then under N_2 for 30 min) or TOPO (previously degassed under vacuum, 50 mbar, at 120° for 30 min, then under N_2 for 30 min) is added to the test tube. To this solution is rapidly injected an amount of 1.5 mmol or 0.5 mmol, or 0.15 mmol or 0.05 mmol of TOP or DPP and the reaction was carried out under N_2. The test tube was immediately put in a stirrer set at the desired temperature (220 °C) for 60 min. During the first 5 minutes the temperature within the pyrex tube drops to 210 °C, then reach once again the selected value.

The reaction was stopped cooling the tube at RT in water, then the mixture is poured in 40 ml of acetone. The QDs grown in TOPO were purified as reported above. The QDs grown in ODE were purified following the same protocol with minor modifications. The reaction mix was stopped in cold water then the solution is poured in 40 ml of acetone. A volume of 2-5 ml of acetonitrile is then added as soon as the solution become cloudy. The solution is then centrifuged at 4000 rpm for 20 minutes. The precipitate is redissolved with 0.2-0.4 ml of chloroform and is transferred in eppendorfs. For a chloroform volume of 0.2 ml it has been added 1.2 ml of acetone/acetonitrile 1:1 (v/v) and the solution is then centrifuged

at 14.000 rpm for 10 minutes. The precipitate was washed once again with 1.2 ml of acetone/acetonitrile 1:1 (v/v) and then the precipitate is resuspended in 0.5 ml of cloroform.

Optical characterisation of the samples: The solutions were analysed both by UV-Vis and PL spectroscopy. The UV-Vis spectra are recorded dissolving a volume (5-50 μl) in 3 ml of chloroform in such a way that the absorption at 350 nm is about 0.1. The same solution is then used to record the PL spectra and to determine the PLQY. The PL spectra were recorded in the region between 400 – 800 nm, with an emission bandwidth of 1.6 nm and exciting the sample at 350 nm with an excitation bandwidth of 1.8, dwell time 0.6 sec and step 1 nm (FSP920 Edinburgh Instruments). The PL spectrum was then corrected by the detector response.

Analysis of the optical data: CdS QDs size determination and size distribution: The FWHM has been determined by using the Origin program converting the WL axis of the absorption spectrum (WL vs Abs) in a new graph where the WL has been changed in QDs size using the Yu et al equation (particle size vs Abs). Then the absorprtion peak of the CdS has been fitted with the Gaussian curve obtaining the FWHM of the particle size. The curve fitting of the particle size and FWHM has been obtained with the asymptotic equation $y = a - b*c^x$. In the case of size the fitting parameters are: “a” = 3.15, “b” = 2.30 and “c” = 0.98 with a R^2 of 0.993. In the case of FWHM the fitting parameters are: “a” = 1.21, “b” = 0.26 and “c” = 0.98 with a R^2 of 0.519.

Thin film preparation and analysis: For optical spectroscopy, thin films of QDs were spin-coated on fused silica substrates. The absorption spectra were measured using a Varian UV spectrophotometer and photoluminescence spectra were measured with a JY Horiba Fluoromax fluorimeter. For devices, ITO-coated soda lime glass substrates were cleaned by ultrasound in acetone and 2-propanol, followed by an oxygen plasma treatment. A 40 nm thick poly(3,4-ethylenedioxythiophene): poly(styrenesulfonate) (PEDOT:PSS) was spin-coated on the ITO and baked on a hot plate at 120 °C for 10 min. A hole-transport layer of 35

nm-thick poly(N-vinylcarbazole) (PVK) was spin-coated on the PEDOT:PSS layer and baked at 80 °C for 2 hours in a nitrogen glove box. An emissive layer of either QDs alone or QDs blended with (4, 4'-N, N'-dicarbazole) biphenyl (CBP) and 4-diphenylphosphoryl dibenzofuran (o-DBFPPO) were spin-coated on top of the PVK layer. An electron-transport layer of 60 nm-thick bis-4,6-(3,5-di-3-pyridylphenyl)-2-methylpyrimidine (B3PyMPM) was deposited through a shadow mask. A cathode of Ca/Al (20 nm/100 nm) was then deposited on the B3PyMPM layer in the same vacuum system. After the evaporation, the devices were encapsulated with optical curing adhesive (Norland NOA68) and glass coverslips in the glove box. The device has an active area of 2x1.5 mm^2. The current-voltage-light output characteristics were measured using a Keithley source measure unit with a calibrated silicon photodiode. The EL spectra were measured using a charge coupled device spectrograph.

Acknowledgements: We acknowledge financial support from FP7 project "Laser Induced Synthesis of Polymeric Nanocomposite Materials and Development of Micro-patterned Hybrid Light Emitting Diodes (LED) and Transistors (LET)"-LAMP project (G. A.247928). AKB and IDWS also acknowledge financial support from EPSRC Programme grant "Challenging the limits of photonics: Structured light" EP/J01771X/1.

Received: ((will be filled in by the editorial staff))
Revised: ((will be filled in by the editorial staff))
Published online: ((will be filled in by the editorial staff))

[1] M.L. Steigerwald, A.P. Alivisatos, J.M. Gibson, T.D. Harris, R. Kortan, A.J. Muller, A.M. Thayer, T.M. Duncan, D.C. Douglass, L.E. Brus, Surface derivatization and isolation of semiconductor cluster molecules, J. Am. Chem. Soc., 110 (1988) 3046-3050.
[2] J.W. Stouwdam, R.A.J. Janssen, Red, green, and blue quantum dot LEDs with solution processable ZnO nanocrystal electron injection layers, J. Mater. Chem., 18 (2008) 1889-1894.
[3] S. Coe, W.-K. Woo, M. Bawendi, V. Bulovic, Electroluminescence from single monolayers of nanocrystals in molecular organic devices, Nature, 420 (2002) 800-803.
[4] L. Qian, Y. Zheng, J. Xue, P.H. Holloway, Stable and efficient quantum-dot light-emitting diodes based on solution-processed multilayer structures, Nat Photon, 5 (2011) 543-548.
[5] J.P. Clifford, G. Konstantatos, K.W. Johnston, S. Hoogland, L. Levina, E.H. Sargent, Fast, sensitive and spectrally tuneable colloidal-quantum-dot photodetectors, Nat Nano, 4 (2009) 40-44.
[6] S. Dayal, N. Kopidakis, D.C. Olson, D.S. Ginley, G. Rumbles, Photovoltaic Devices with a Low Band Gap Polymer and CdSe Nanostructures Exceeding 3% Efficiency, Nano Letters, 10 (2009) 239-242.
[7] M. Bruchez, M. Moronne, P. Gin, S. Weiss, A.P. Alivisatos, Semiconductor Nanocrystals as Fluorescent Biological Labels, Science, 281 (1998) 2013-2016.
[8] E. Jang, S. Jun, H. Jang, J. Lim, B. Kim, Y. Kim, White-Light-Emitting Diodes with Quantum Dot Color Converters for Display Backlights, Adv. Mater., 22 (2010) 3076-3080.
[9] B.S. Mashford, M. Stevenson, Z. Popovic, C. Hamilton, Z. Zhou, C. Breen, J. Steckel, V. Bulovic, M. Bawendi, S. Coe-Sullivan, P.T. Kazlas, High-efficiency quantum-dot light-emitting devices with enhanced charge injection, Nat Photon, 7 (2013) 407-412.
[10] J.M. Pietryga, R.D. Schaller, D. Werder, M.H. Stewart, V.I. Klimov, J.A. Hollingsworth, Pushing the Band Gap Envelope: Mid-Infrared Emitting Colloidal PbSe Quantum Dots, J. Am. Chem. Soc., 126 (2004) 11752-11753.
[11] M.A. Hines, G.D. Scholes, Colloidal PbS Nanocrystals with Size-Tunable Near-Infrared Emission: Observation of Post-Synthesis Self-Narrowing of the Particle Size Distribution, Adv. Mater., 15 (2003) 1844-1849.
[12] J.R. Sommer, R.T. Farley, K.R. Graham, Y. Yang, J.R. Reynolds, J. Xue, K.S. Schanze, Efficient Near-Infrared Polymer and Organic Light-Emitting Diodes Based on Electrophosphorescence from (Tetraphenyltetranaphtho[2,3]porphyrin)platinum(II), ACS Applied Materials & Interfaces, 1 (2009) 274-278.
[13] L. Sun, J.J. Choi, D. Stachnik, A.C. Bartnik, B.-R. Hyun, G.G. Malliaras, T. Hanrath, F.W. Wise, Bright infrared quantum-dot light-emitting diodes through inter-dot spacing control, Nat Nano, 7 (2012) 369-373.
[14] K.N. Bourdakos, D.M.N.M. Dissanayake, T. Lutz, S.R.P. Silva, R.J. Curry, Highly efficient near-infrared hybrid organic-inorganic nanocrystal electroluminescence device, Applied Physics Letters, 92 (2008) -.
[15] M.G. Vander Heiden, Targeting cancer metabolism: a therapeutic window opens, Nat Rev Drug Discov, 10 (2011) 671-684.
[16] W.S. Rees, G. Kräuter, Preparation and characterization of several group 12 element (Zn, Cd)-bis(thiolate) complexes and evaluation of their potential as precursors for 12–16 semiconducting materials, Journal of Materials Research, 11 (1996) 3005-3016.
[17] D.V. Talapin, J.-S. Lee, M.V. Kovalenko, E.V. Shevchenko, Prospects of Colloidal Nanocrystals for Electronic and Optoelectronic Applications, Chem. Rev., 110 (2009) 389-458.
[18] F. Silva, M. Carvalho, R. Mendonca, W. Macedo, K. Balzuweit, P. Reiss, M. Schiavon, Effect of surface ligands on the optical properties of aqueous soluble CdTe quantum dots, Nanoscale Research Letters, 7 (2012) 536.

[19] W.W. Yu, L. Qu, W. Guo, X. Peng, Experimental Determination of the Extinction Coefficient of CdTe, CdSe, and CdS Nanocrystals, Chemistry of Materials, 15 (2003) 2854-2860.
[20] F. Wang, V.N. Richards, S.P. Shields, W.E. Buhro, Kinetics and Mechanisms of Aggregative Nanocrystal Growth, Chemistry of Materials, 26 (2013) 5-21.
[21] X. Peng, J. Wickham, A.P. Alivisatos, Kinetics of II-VI and III-V Colloidal Semiconductor Nanocrystal Growth: "Focusing" of Size Distributions, J. Am. Chem. Soc., 120 (1998) 5343-5344.
[22] H.H.-Y. Wei, C.M. Evans, B.D. Swartz, A.J. Neukirch, J. Young, O.V. Prezhdo, T.D. Krauss, Colloidal Semiconductor Quantum Dots with Tunable Surface Composition, Nano Letters, 12 (2012) 4465-4471.
[23] N.C. Anderson, M.P. Hendricks, J.J. Choi, J.S. Owen, Ligand Exchange and the Stoichiometry of Metal Chalcogenide Nanocrystals: Spectroscopic Observation of Facile Metal-Carboxylate Displacement and Binding, J. Am. Chem. Soc., 135 (2013) 18536-18548.
[24] S. Leubner, R. Schneider, A. Dubavik, S. Hatami, N. Gaponik, U. Resch-Genger, A. Eychmuller, Influence of the stabilizing ligand on the quality, signal-relevant optical properties, and stability of near-infrared emitting Cd1-xHgxTe nanocrystals, Journal of Materials Chemistry C, 2 (2014) 5011-5018.
[25] A.L. Rogach, T. Franzl, T.A. Klar, J. Feldmann, N. Gaponik, V. Lesnyak, A. Shavel, A. Eychmüller, Y.P. Rakovich, J.F. Donegan, Aqueous Synthesis of Thiol-Capped CdTe Nanocrystals: State-of-the-Art, The Journal of Physical Chemistry C, 111 (2007) 14628-14637.
[26] S. Dolai, P.R. Nimmala, M. Mandal, B.B. Muhoberac, K. Dria, A. Dass, R. Sardar, Isolation of Bright Blue Light-Emitting CdSe Nanocrystals with 6.5 kDa Core in Gram Scale: High Photoluminescence Efficiency Controlled by Surface Ligand Chemistry, Chemistry of Materials, 26 (2013) 1278-1285.
[27] K.B. Subila, G. Kishore Kumar, S.M. Shivaprasad, K. George Thomas, Luminescence Properties of CdSe Quantum Dots: Role of Crystal Structure and Surface Composition, The Journal of Physical Chemistry Letters, 4 (2013) 2774-2779.
[28] C. Bullen, P. Mulvaney, The Effects of Chemisorption on the Luminescence of CdSe Quantum Dots, Langmuir, 22 (2006) 3007-3013.
[29] C.M. Evans, M.E. Evans, T.D. Krauss, Mysteries of TOPSe Revealed: Insights into Quantum Dot Nucleation, J. Am. Chem. Soc., 132 (2010) 10973-10975.
[30] K. Yu, A. Hrdina, X. Zhang, J. Ouyang, D.M. Leek, X. Wu, M. Gong, D. Wilkinson, C. Li, Highly-photoluminescent ZnSe nanocrystalsvia a non-injection-based approach with precursor reactivity elevated by a secondary phosphine, Chemical Communications, 47 (2011) 8811-8813.
[31] F. Wang, W.E. Buhro, Morphology Control of Cadmium Selenide Nanocrystals: Insights into the Roles of Di-n-octylphosphine Oxide (DOPO) and Di-n-octylphosphinic Acid (DOPA), J. Am. Chem. Soc., 134 (2012) 5369-5380.
[32] F. Wang, R. Tang, W.E. Buhro, The Trouble with TOPO; Identification of Adventitious Impurities Beneficial to the Growth of Cadmium Selenide Quantum Dots, Rods, and Wires, Nano Letters, 8 (2008) 3521-3524.
[33] S.K. Haram, B.M. Quinn, A.J. Bard, Electrochemistry of CdS Nanoparticles: A Correlation between Optical and Electrochemical Band Gaps, J. Am. Chem. Soc., 123 (2001) 8860-8861.
[34] C. Han, G. Xie, H. Xu, Z. Zhang, D. Yu, Y. Zhao, P. Yan, Z. Deng, Q. Li, S. Liu, Towards Highly Efficient Blue-Phosphorescent Organic Light-Emitting Diodes with Low Operating Voltage and Excellent Efficiency Stability, Chemistry – A European Journal, 17 (2011) 445-449.

[35] H.S. Daisaku Tanaka, Yan-Jun Li1, Shi-Jian Su, Takashi Takeda1 and Junji Kido, Ultra High Efficiency Green Organic Light-Emitting Devices, Japanese Journal of Applied Physics 46 (2007) L10-12.
[36] Y. Kobayashi, T. Nishimura, H. Yamaguchi, N. Tamai, Effect of Surface Defects on Auger Recombination in Colloidal CdS Quantum Dots, The Journal of Physical Chemistry Letters, 2 (2011) 1051-1055.

Figures

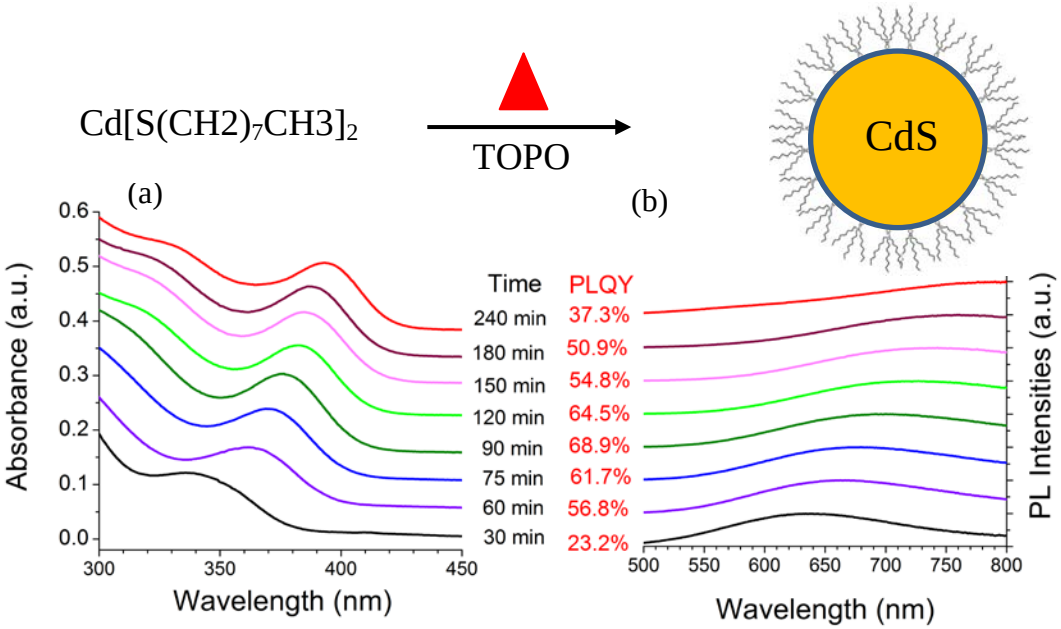

Figure 1: (a) Absorbance and (b) photoluminescence spectra of the TOPO capped cadmium sulfide QDs in solutions at various times during synthesis. The sample was excited at 380 nm. The figure also show the chemical formula of the precursors and representation of TOPO capped QDs after thermolysis.

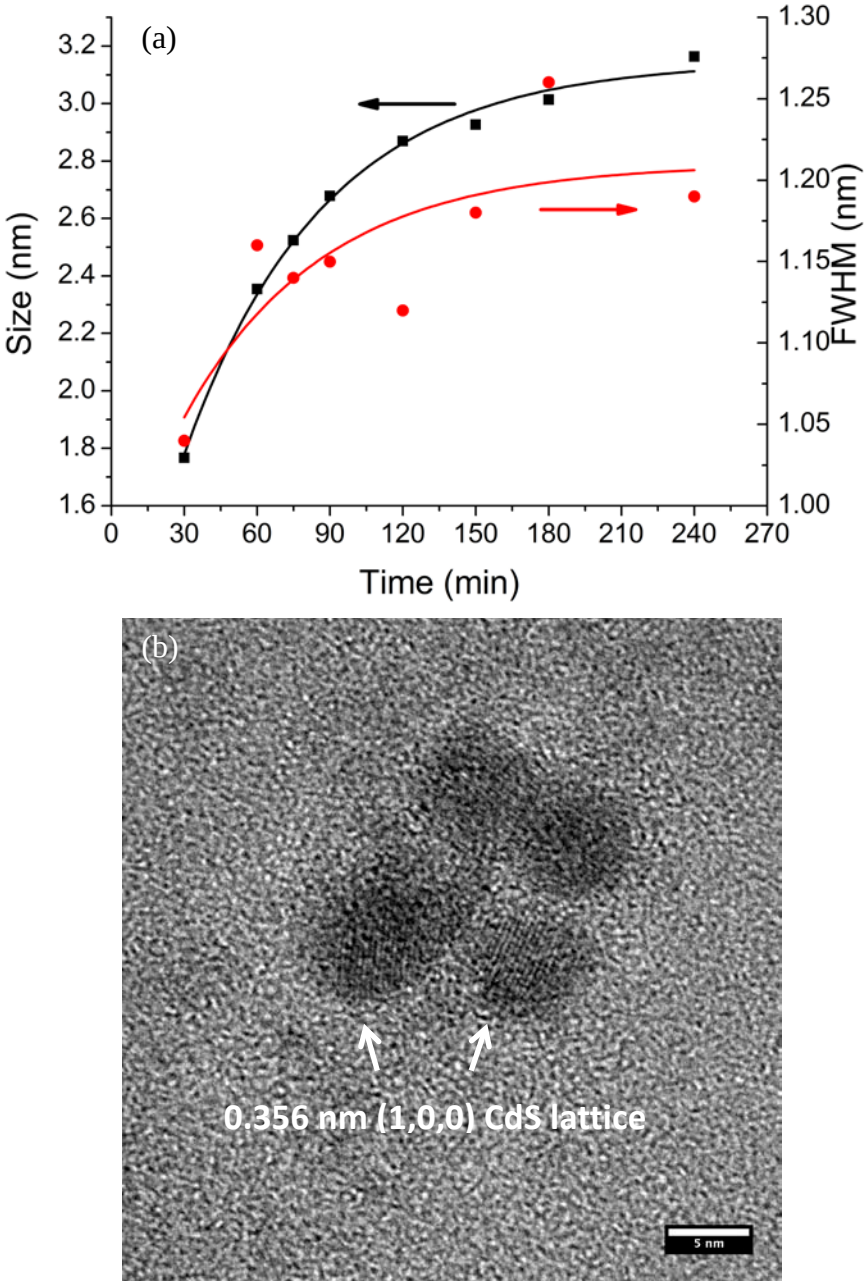

Figure 2: (a) Size (black square experimental values, black line asymptotic fitting) and FWHM (red dot experimental values, red line asymptotic fitting) trend of the CdS growth from cadmium octanthiol at 220° C. (b) TEM image of CdS nanoparticles.

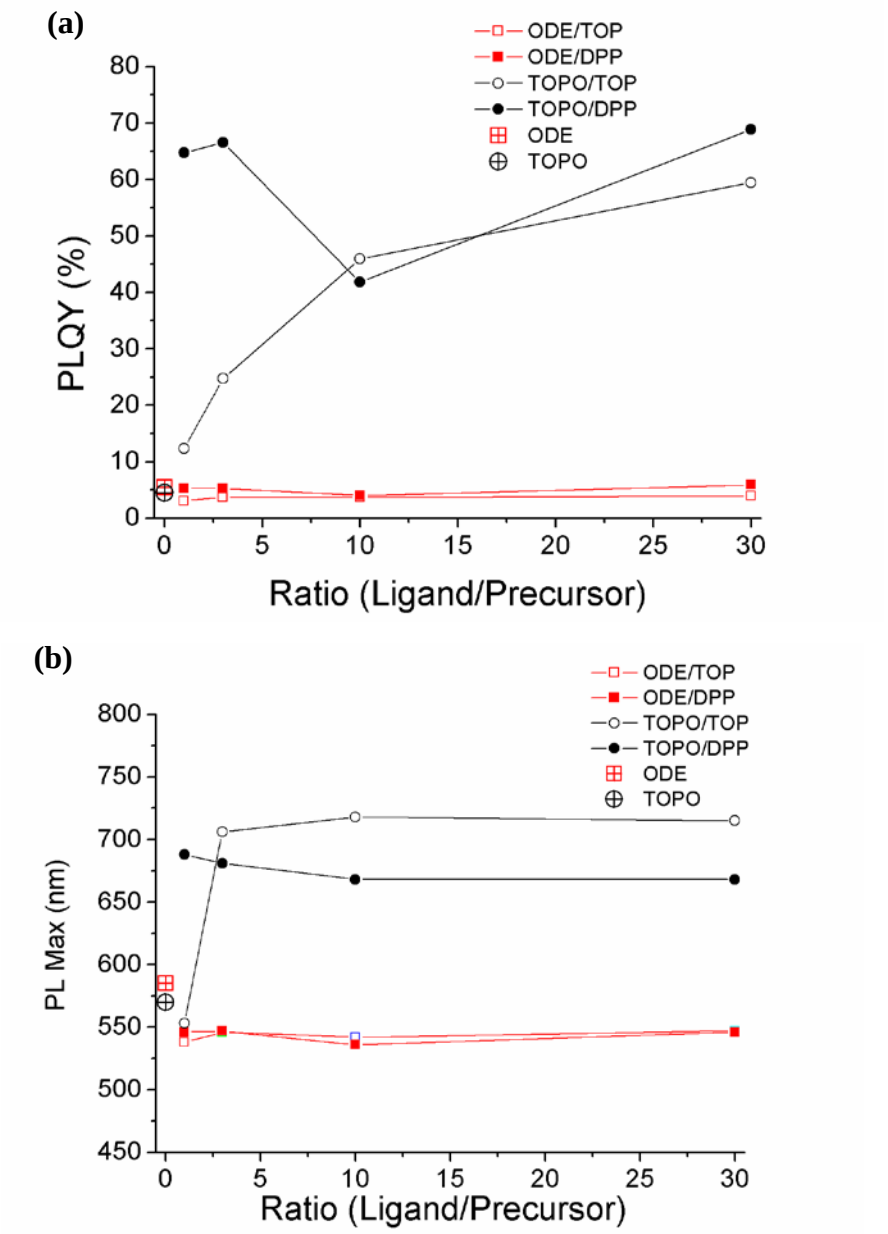

Figure 3. a) PLQY values of CdS QDs prepared at 90°C as a function of ligand/precursor ratio, solvent type (ODE and TOPO) and ligand (TOP and DPP); b) emission maxima of the CdS QDs as a function of ligand/precursor ratio, solvent type (ODE and TOPO) and lingand (TOP and DPP).

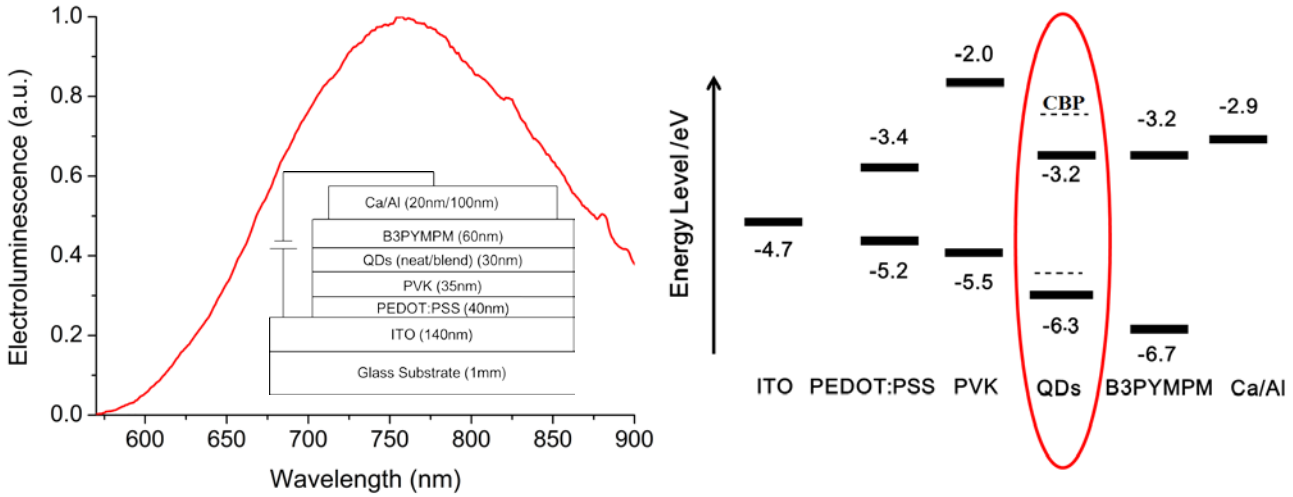

Figure 4. Diagram showing the OLED device structure and corresponding energy levels of various layers together with electroluminescence spectra.

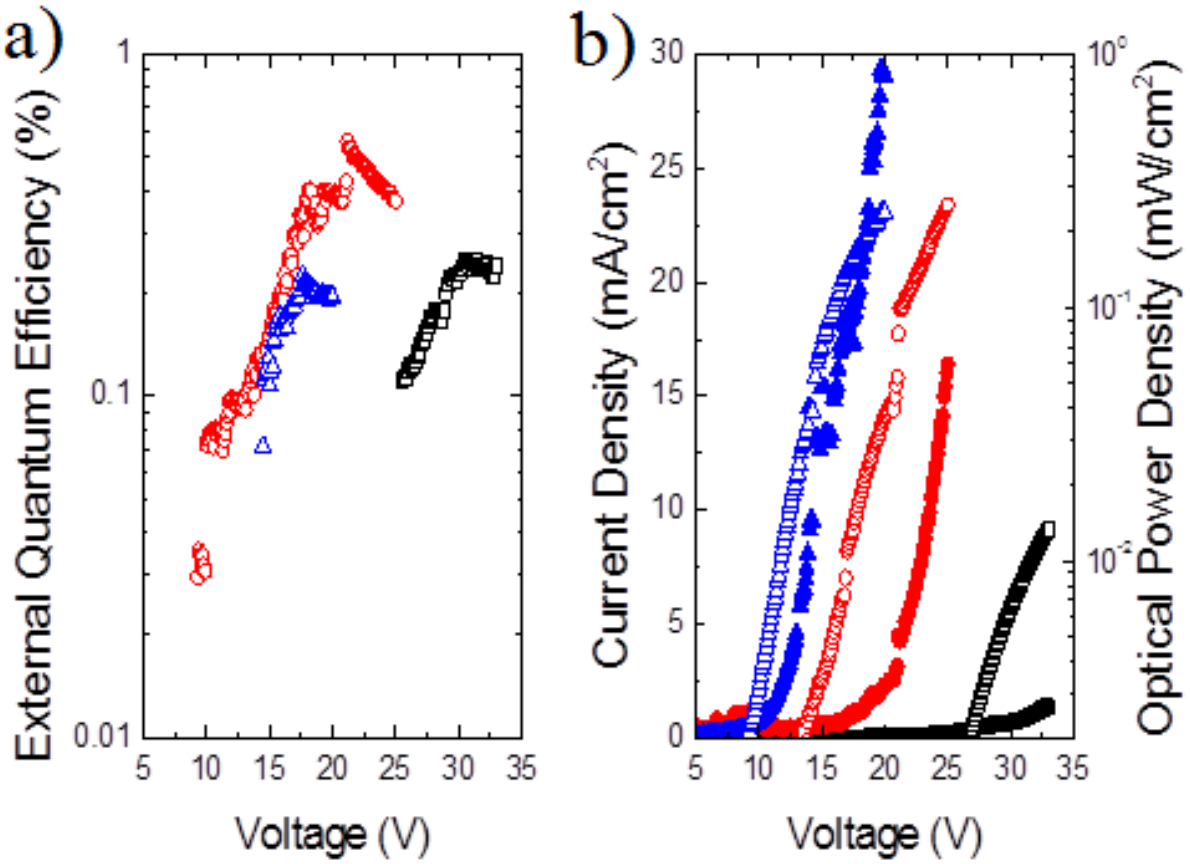

Figure 5. a) External quantum efficiency as a function of the drive voltage. Black squares are for devices with neat quantum dots as the emissive layer (set 1), red circles are for devices with quantum dots:CBP blend as the emissive layer (set 2), blue triangles are for devices with quantum dots:o-DBFPPO blend as the emissive layer (set 3)). b) Current density and optical power density as a function of the driven voltage (solid dots represent the current density, hollow dots represent the optical power density).